AGU PUBLICATIONS

Geophysical Research Letters

RESEARCH LETTER
10.1002/2014GL062402

Key Points:
- We present a procedure to improve geoid models using ocean topography estimates
- Ocean topography products can correct geoid models
- The uncertainty of ocean topography measurements in this region is given

Supporting Information:
- Readme
- Text S1
- Data File S1

Correspondence to:
M. R. Mazloff,
mmazloff@ucsd.edu

Citation:
Mazloff, M. R., S. T. Gille, and B. Cornuelle (2014), Improving the geoid: Combining altimetry and mean dynamic topography in the California coastal ocean, *Geophys. Res. Lett.*, *41*, 8944–8952, doi:10.1002/2014GL062402.

Received 3 NOV 2014
Accepted 20 NOV 2014
Accepted article online 25 NOV 2014
Published online 16 DEC 2014

Improving the geoid: Combining altimetry and mean dynamic topography in the California coastal ocean

Matthew R. Mazloff[1], Sarah T. Gille[1], and Bruce Cornuelle[1]

[1]Scripps Institution of Oceanography, University of California, San Diego, La Jolla, California, USA,

Abstract Satellite gravity mapping missions, altimeters, and other platforms have allowed the Earth's geoid to be mapped over the ocean to a horizontal resolution of approximately 100 km with an uncertainty of less than 10 cm. At finer resolution this uncertainty increases to greater than 10 cm. Achieving greater accuracy requires accurate estimates of the dynamic ocean topography (DOT). In this study two DOT estimates for the California Current System with uncertainties less than 10 cm are used to solve for a geoid correction field. The derived field increases the consistency between the DOTs and along-track altimetric observations, suggesting it is a useful correction to the gravitational field. The correction is large compared to the dynamic ocean topography, with a magnitude of 15 cm and significant structure, especially near the coast. The results are evidence that modern high-resolution dynamic ocean topography products can be used to improve estimates of the geoid.

1. Introduction

Satellite measurements from the Gravity Recovery and Climate Experiment (GRACE) and the Gravity Field and Steady-State Ocean Circulation Explorer (GOCE) provide a method for determining the Earth's gravity potential or geoid [*Rapp*, 1998]. These satellite gravity measurements yield estimates of the spherical harmonic coefficients of the Earth's gravitational field accurate to a few centimeters up to approximately degree and order 250 or to approximately 80 km at the equator [*Pail et al.*, 2011]. The Earth's geoid, however, has significant structure at smaller spatial scales. Because the geodetic satellites fly 250 to 500 km above the Earth's surface, shorter length scales are attenuated and cannot be determined. Terrestrial observations and satellite altimetry are used to determine the geoid at higher resolution, but terrestrial observations are geographically limited, and satellite altimetry does not distinguish sea surface height (SSH) undulations associated with ocean circulation from undulations associated with the geoid. This inability to distinguish the components diminishes the oceanographic utility of altimeters with long repeat period orbits. However, the ability to utilize these measurements is critical given the growing constellation of altimeters with varying orbits and the coming wide-swath altimeters. In this paper we implement a method for improving geoid estimates over the ocean on scales below 200 km, relying primarily on information from high-precision satellite altimeters and a priori knowledge of the ocean circulation. Using the California Current System as a regional test bed, we suggest that this method can pave the way for better oceanographic use of long-repeat altimeter data.

Satellite altimeters measure their height above the ocean surface at horizontal spatial scales of order 10 km, showing ~100 m undulations relative to the reference ellipsoid. If the ocean were at rest, its surface would lie on an equipotential surface, the geoid, and altimetric SSH would directly measure the geoid. In reality, the mean sea surface height, ⟨SSH⟩, can differ from the geoid by 1 m or more, and the difference, ⟨SSH⟩ minus geoid undulation, is the mean dynamic ocean topography ⟨DOT⟩ [e.g., *Hughes and Bingham*, 2008]. Separating this DOT signal from the geoid is challenging.

The Earth Gravitational Model 2008 (EGM2008); [*Pavlis et al.*, 2012] was estimated to degree 2190 and order 2159 through an iterative least squares adjustment procedure that ensures consistency with a GRACE-only gravitational model while reducing the residuals between SSH observations and a mean dynamic ocean topography. The ⟨DOT⟩ is determined as part of the iterative process by differencing the updated gravitational model from a mean sea surface product [*Andersen and Knudsen*, 2009] and is therefore a product of the optimization. This is a common practice; to date, improved knowledge of the geoid has come primarily through dedicated gravity missions and has led to improved knowledge of the mean DOT [e.g., *Tai and Wunsch*, 1983; *Zlotnicki and Marsh*, 1989; *Nerem et al.*, 1990; *Tapley et al.*, 2003; *Knudsen et al.*, 2011;

Volkov and Zlotnicki, 2012; *Bingham et al.*, 2014]. A gravitational model can also be determined, however, by differencing SSH observations from a DOT estimate, time averaging, and then spatially filtering. Thus, improved knowledge of the DOT has the capability to improve knowledge of the geoid. This has long been recognized; determining the best geoid estimate requires a full synthesis of geodetic and oceanographic information [*Wunsch and Gaposchkin*, 1980; *Ganachaud et al.*, 1997]. Here we build on the concepts presented in these previous works and evaluate whether modern high-resolution DOT products can be used to infer useful geoid corrections in the region of the California Current System.

Determining the DOT from limited observations of the ocean circulation is not a trivial task [*Maximenko et al.*, 2009]. We do, however, know the dynamical constraints (i.e., the Navier-Stokes equations) governing the system, and observations provide other constraints on the circulation. Two estimates of DOT are used in this work. One is derived from mapped altimetry [*Ducet et al.*, 2000] and other sources [*Rio et al.*, 2011]. A second is derived using the adjoint method [*Wunsch and Heimbach*, 2013] to bring a model DOT into consistency with all available observations while obeying the discretized Navier-Stokes equations as represented by the Massachusetts Institute of Technology general circulation ocean model (MITgcm) [*Marshall et al.*, 1997]. We then combine these estimates of the DOT with altimetry to infer a correction field to EGM2008. We show that this corrected geoid is more consistent with SSH observations for all altimeters and over all time, even those not used in determining the correction. The correction product is publicly available as supporting information.

2. Estimating the Dynamic Ocean Topography

A state estimate of the California Current System has been produced for the period 1 January 2007 to 31 December 2010 using the adjoint method as implemented by the consortium for Estimating the Circulation and Climate of the Ocean [*Stammer et al.*, 2002; *Wunsch and Heimbach*, 2013]. The MIT general circulation ocean model (MITgcm) is configured at 1/16° horizontal resolution and with 72 vertical levels of variable thickness in a domain extending from 27.2°N to 40°N and from 130°W to the coast. The inputs to this model (initial conditions, open boundary conditions, and prescribed atmospheric state) are then adjusted in an iterative process that brings the solution into consistency with in situ measurements of temperature and salinity and with satellite measurements of along-track sea surface height and temperature. A constraint to EGM2008 is implemented, though we find that this has a small effect on the optimized solution due to a large prescribed uncertainty. Earlier versions of this state estimate were presented by *Todd et al.* [2011] and by *Verdy et al.* [2014]. *Todd et al.* [2012] showed that the solution resolves ocean structures with scales greater than 30 km. Here we use a solution denoted as iteration 186.

The 2007–2010 mean dynamic ocean topography, $\langle \mathrm{DOT} \rangle$, drops from west to east providing the surface pressure gradient balancing the geostrophic California Current (Figure 1a). The drop is greatest in the southern portion of the study domain. Here the SSH change is ∼20 cm and the mean southward transport is ∼5 Sv.

The methodology (described below) to solve for a geoid correction field is also carried out using the Archiving, Validation, and Interpretation of Satellite Oceanographic data (AVISO) Mapped Absolute Dynamic Topography product (Figure 1b). These maps were produced by Ssalto/Duacs and distributed by AVISO, with support from Centre National d'Etudes Spatiales (CNES) (http://www.aviso.oceanobs.com/duacs/). Delayed time mode data were used and at the time of analysis were available as daily snapshots at 7 day intervals from 14 October 1992 to 7 August 2013. Like the state estimate, the AVISO product is informed by gravity data from the GRACE mission. The nominal resolution of this product is 1/3°, and it is filtered to suppress structures at length scales shorter than approximately 100 km. The AVISO 2007–2010 $\langle \mathrm{DOT}_{\mathrm{AV}} \rangle$ differs from the state estimate $\langle \mathrm{DOT}_{\mathrm{SE}} \rangle$ (Figure 1c). These differences, which have a maximum of 7.1 cm and a root-mean-square (RMS) of 2.1 cm, are an indicator of the uncertainty in the estimated mean dynamic ocean topography.

The largest differences in the $\langle \mathrm{DOT} \rangle$ estimates are in the northwest and southeast parts of the domain (Figure 1c). The northwest is the most poorly observationally constrained region of the state estimate. In addition, it is near the open-ocean boundary condition for the inflowing California Current, which is not certain to be reliable. Thus, the AVISO product may be more accurate in the northwest region. The southeast region, however, is better constrained by observations from the California Cooperative Oceanic Fisheries Investigations (CalCOFI), Spray glider lines, and moorings [*Todd et al.*, 2012; *Ohman et al.*, 2013]. Furthermore,

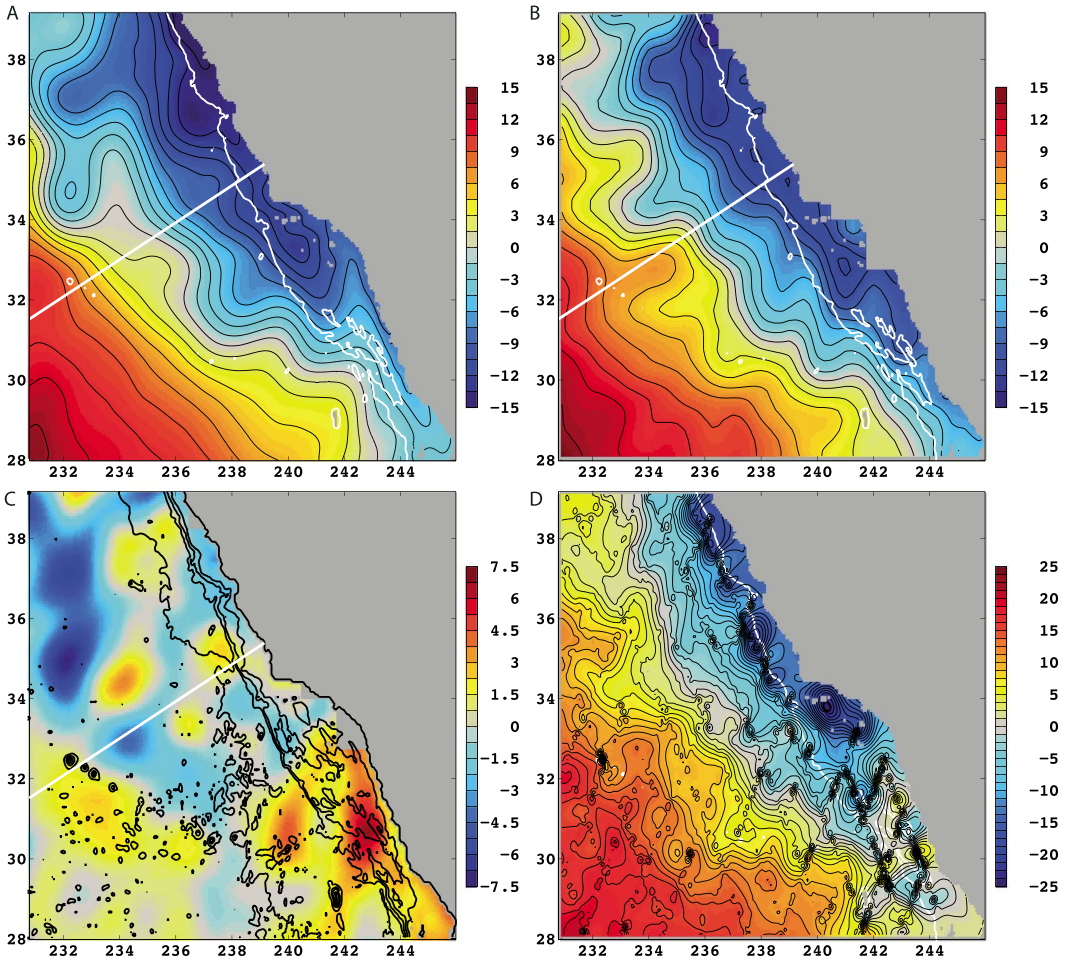

Figure 1. Mean dynamic ocean topography from the (a) state estimate and (b) AVISO for 2007–2010. Contour interval is 1.5 cm. The 2000 m bathymetric contour and CalCOFI line 75 are shown in white. (c) The state estimate $\langle DOT_{SE} \rangle$ minus the AVISO $\langle DOT_{AV} \rangle$. Bathymetry is contoured in black with a 1000 m interval. (d) The state estimate mean dynamic topography plus the geoid correction field ($\langle DOT_{SE} \rangle + F_{SE}$). As in Figures 1a and 1b the contour interval is 1.5 cm, and the 2000 m bathymetric contour is shown in white. The field $\langle DOT_{AV} \rangle + F_{AV}$ looks similar.

the complex topography and coastal waveguide are expected to be problematic for the AVISO product. For these reasons the state estimate is hypothesized to be more accurate in the southeast. The regions of differing $\langle DOT \rangle$ estimates are examined separately in the analysis below using the CalCOFI line 75 as the boundary (white line in Figures 1a–1c and 2a and 2b).

3. Calculating the Geoid Correction Field

The geoid model, the SSH observations, and the DOT estimate all have significant uncertainties. We therefore define an initial residual field, r_i = SSH − DOT − geoid. As we will show in section 3.1, at the length scales we are considering (i.e., less than 200 km) the uncertainties in the geoid are larger than uncertainties in the DOT, and thus, we seek to determine a geoid correction field, F, that minimizes r_i. Our method entails first calculating r_i at observation points using only exact repeat altimeters that were assimilated into the state estimate and then objectively mapping r_i to determine a continuous geoid correction. These two activities are described in detail in the supporting information. Here we summarize only the main points regarding the mapping. The uncertainty prescribed to the time-averaged residuals, $\sigma_r = (400\ \text{cm}^2/N + 4\ \text{cm}^2)$, depends on the number, N, of repeat SSH observations and averages about 3 cm for most locations. The geoid error covariance used to map the residuals is the sum of three Gaussians with e-folding distances of 10 km, 60 km, and 250 km and amplitudes 9 cm^2, 25 cm^2, and 25 cm^2, respectively.

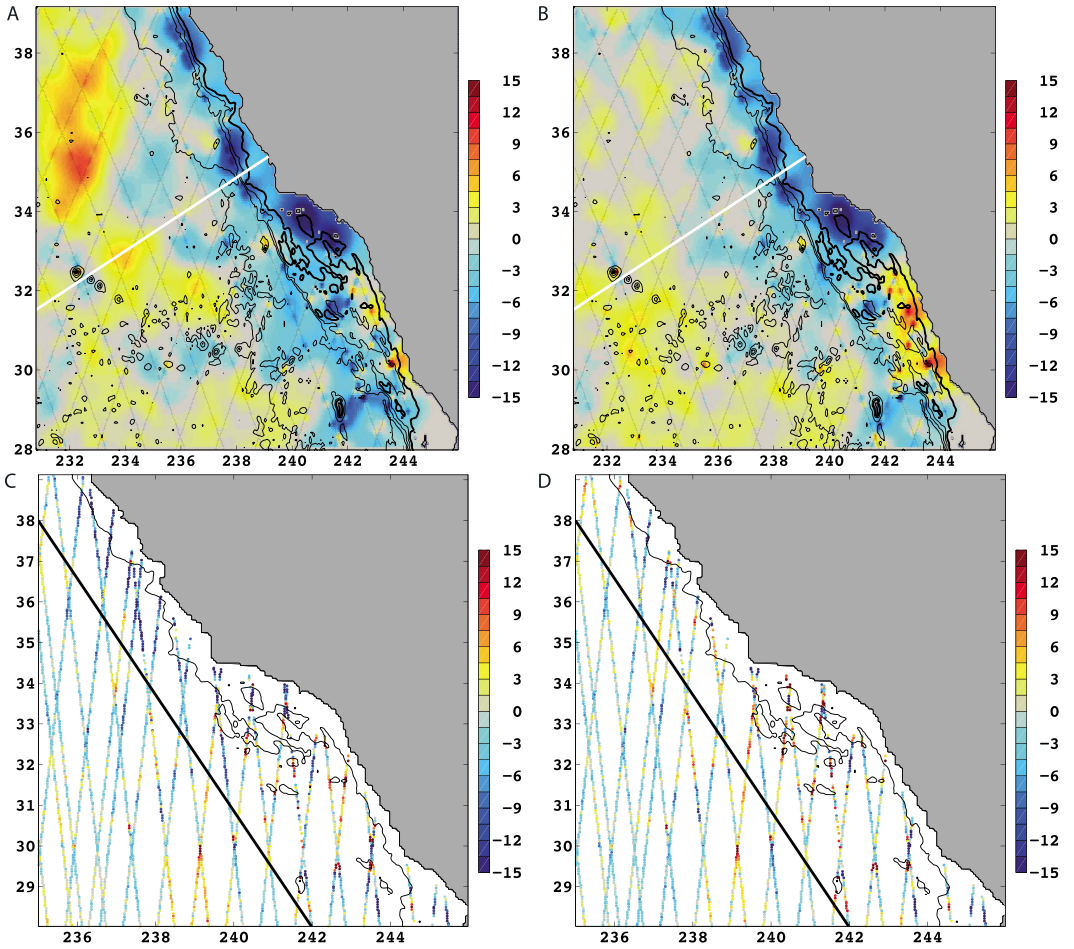

Figure 2. The geoid correction field, *F*, in centimeters from the (a) state estimate and (b) AVISO. As in Figure 1c the bathymetry is contoured in black with a 1000 m contour interval, and the CalCOFI line 75 is shown in white. The difference between these two panels looks similar to Figure 1c. The (c) initial and (d) corrected residuals between the AVISO DOT, EGM2008, and CryoSat-2 for July 2012 in centimeters. The 1000 m bathymetry contour is denoted with a thin black line. The geoid correction is most influential shoreward of the thick black line, where it reduces the RMS of the residuals from 9.2 cm to 7.3 cm. Note that the longitude axes are different for Figures 2a and 2b and 2c and 2d.

Thus, the total error variance prescribed on the geoid is 59 cm^2, which is consistent with the claim that EGM2008 should allow determination of a DOT that is accurate to ~7 cm [*Pavlis et al.*, 2012].

As discussed in the supporting information, the mapping residuals have a distribution with a kurtosis greater than Gaussian. The spatial distribution of these residuals reveals that the largest values are found around complex bathymetry (not shown). It is likely that our prescribed mapping uncertainty is too large over much of the domain but too small in the vicinity of complex bathymetry. However, a tight correlation was not found between the residuals and either depth or bathymetric gradient. Future work should determine a better method for determining uncertainty that accounts for topographic structure and thus allows for anisotropic and inhomogeneous covariances and a reduction in the prescribed noise over the deep and flat-bottom regions.

The mapped geoid correction fields (Figures 2a and 2b) exhibit both large-scale and small-scale structures. The large-scale structure is high to the east and low along the coast. The slope of the correction is clearest in the region just south of CalCOFI line 75, where it is greater than 10 cm across the region. The small-scale structures are found primarily around complex topography, implying correction to the slope of these features. However, the lack of resolution in the DOT product does call into question the accuracy of the

corrections at the shortest wavelengths. Differences in the correction fields calculated using either the state estimate or the AVISO product reflect differences in the mean DOTs (Figure 1c).

3.1. A Posteriori Evaluation of Geoid Correction Field

We have mapped a field, F, with length scales of approximately 10 km to 250 km that minimizes the 2007–2010 mean structure in $\langle r_c \rangle = \langle \mathrm{SSH} - \mathrm{DOT} - \mathrm{geoid} - F \rangle$, where SSH is taken from the Jason altimeters. In the following section we will show that the correction, F, reduces the RMS of the residuals, r_c, for all altimeters and time. Mathematically, however, F could be attributed to either errors in the $\langle \mathrm{DOT} \rangle$ or in the geoid. A priori we hypothesized that F is more likely to represent geoid error than DOT error. An a posteriori check of this is to assume a perfect geoid and evaluate the realism of the $\langle \mathrm{DOT} \rangle$ that would result if this correction field, F, was added to the state estimate or AVISO $\langle \mathrm{DOT} \rangle$. The mean dynamic ocean topography from AVISO and the state estimate show significant differences (Figure 1c). The respective correction fields, however, compensate for these differences such that the state estimate ($\langle \mathrm{DOT} \rangle_{\mathrm{SE}} + F_{\mathrm{SE}}$) is approximately equal to the AVISO-derived ($\langle \mathrm{DOT} \rangle_{\mathrm{AV}} + F_{\mathrm{AV}}$). Both these fields imply an unphysical surface topography (Figure 1d). While the dynamic range for the AVISO and state estimate $\langle \mathrm{DOT} \rangle$ is approximately 31 cm in this domain (Figure 1), the ($\langle \mathrm{DOT} \rangle + F$) field has a dynamic range of 55 cm and thus implies a much more energetic California Current System than is observed. Glider observations of CalCOFI line 80 and line 90, which are parallel to line 70 shown in Figure 1 but each offset to the south by ~2.3° of latitude, show instantaneous surface speeds reaching 30 cm s^{-1}. The time mean speeds, however, do not exceed 15 cm s^{-1} [*Todd et al.*, 2011]. Considering the whole domain, surface geostrophic velocities in the state estimate and AVISO mean dynamic ocean topography average 4 cm s^{-1}, with maximum speeds of about 13 cm s^{-1}. The mean surface geostrophic speeds implied from the adjusted $\langle \mathrm{DOT} \rangle$ often exceed 30 cm s^{-1}, which are too large to be realistic [*Lynn and Simpson*, 1987]. Furthermore, the adjusted $\langle \mathrm{DOT} \rangle$ implies substantial time average recirculations just off the California coast. Interpretation at these length scales requires caution because, as noted above, the AVISO and state estimate products only resolve ocean structures greater than ~66 km and ~30 km, respectively. Nevertheless, the magnitude of these corrections are too large to be interpreted as time-mean unresolved ocean features in this region [*Davis et al.*, 2008; *Gay and Chereskin*, 2009; *Todd et al.*, 2011]. Thus, while our method does not distinguish geoid errors from $\langle \mathrm{DOT} \rangle$ errors, physical arguments support the hypothesis that the correction can be primarily attributed to uncertainty in the geoid. Moreover, the magnitude of the correction is within the estimated ~16 cm uncertainty for the geoid at length scales shorter than 133 km estimated by *Bingham et al.* [2014].

4. Evaluating the Geoid Correction Field

The quality of the geoid correction field, F, is determined by quantifying the impact it has on reducing r_c for independent observations and thus bringing the geoid into consistency with SSH and DOT estimates. The following describes the fields used in the evaluations and their nomenclature:

1. Sea surface height (SSH). Along-track observations of sea surface height are obtained from the Radar Altimeter Database System (http://rads.tudelft.nl), which comprises exact repeat and nonrepeat altimeters, including TOPEX (TX), Poseidon (PN), ERS-2 (E2), GFO-1 (G1), Jason-1 (J1), Jason-2 (J2), CryoSat-2 (C2), and SARAL/AltiKa (SA).
2. Mean sea surface height (DTU10). The global mean sea surface product known as DTU10 (see http://www.space.dtu.dk/english/Research/Scientific_data_and_models/Global_Mean_sea_surface) is obtained by mapping SSH observations over the years 1993–2009.
3. Geoid. The Earth Gravitational Model EGM2008 to degree 2190 and order 2159 (http://earth-info.nga.mil/GandG/wgs84/gravitymod/egm2008/index.html). Newer geoid models that include measurements from the Gravity Field and Steady-State Ocean Circulation Explorer (GOCE) satellite are available but are not considered here as GOCE has yet to provide significant improvement at spherical harmonic degrees higher than ~250 [*Pail et al.*, 2011].
4. Dynamic ocean topography (DOT = $\langle \mathrm{DOT} \rangle$ + DOT'). $\mathrm{DOT}_{\mathrm{SE}}$ is derived from iteration 186 of the state estimate. It is available for 2007–2010 at http://sose.ucsd.edu/CASE. $\mathrm{DOT}_{\mathrm{AV}}$ is the AVISO Mapped Absolute Dynamic Topography produced by Ssalto/Duacs and distributed by AVISO, with support from CNES (http://www.aviso.oceanobs.com/duacs/). The mean dynamic topography, $\langle \mathrm{DOT}_{\mathrm{AV}} \rangle$, was calculated over the 2007–2010 period when the state estimate was available.

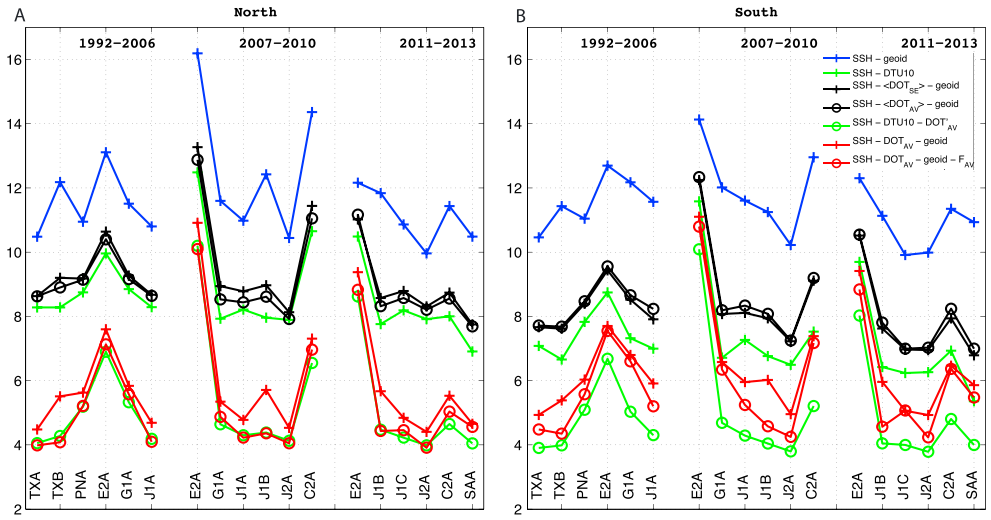

Figure 3. RMS residuals for the (a) northern and (b) southern region in centimeters. The analysis has been separated into the period before the assimilation (1992–2006), during the assimilation (2007–2010), and after the assimilation (2011–2013). The geoid correction, *F*, is determined only using data during the assimilation period. The blue line is SSH − geoid and thus excludes the DOT. The black lines include the mean dynamic ocean topography from the state estimate (plus signs) and from AVISO (circles) but neglect ocean variability. The upper green line is SSH minus DTU10 and thus also excludes ocean variability. The lower green line accounts for ocean variability using the AVISO DOT′. The red lines also account for ocean variability using the AVISO DOT. The upper red line compares SSH minus DOT to the EGM2008 geoid, while the lower line uses the corrected EGM2008 geoid. The *x* axis denotes the altimeter used with nomenclature as described in the text. The third character in the name denotes mission phase (e.g., J1B denotes the Jason-1 altimeter phase B). All the altimeters have relatively short orbit repeat periods except J1C, C2A, and SAA.

5. Geoid correction field (*F*). F_{SE} and F_{AV} are corrections to EGM2008 geoid derived using J1, J2, and DOT_{SE} and DOT_{AV}, respectively. Both are determined using the same methodology and over the same time period and spatial domain.

Using these fields, we calculate the RMS of r_c = SSH − DOT − geoid − *F* for various permutations. We do this for all altimeters, including those not assimilated, and for periods before the state estimate, during the state estimate, and after the state estimate. For each permutation a constant offset was removed to minimize the discrepancy. This offset is unconstrained and irrelevant in this calculation as only the sea surface gradient is of dynamical consequence.

4.1. Importance of the DOT

First, we gauge the impact of the DOT by assuming it to be negligible and calculating RMS(SSH − geoid). The RMS difference of ∼11 cm is an estimate of the uncertainty that one would attribute to the geoid in this region if it were derived directly from altimetry without accounting for ocean structure (blue line in Figure 3).

4.2. Importance of the Time-Varying DOT

We gauge the uncertainty that can be attributed to the time variable mesoscale dynamics in the DOT by determining RMS(SSH − DTU10). For this case we find the RMS to be approximately 9 cm in the northern domain and 7 cm in the southern domain (upper green line in Figure 3). In principle, DTU10 should equal ⟨DOT⟩ + geoid, and thus, we expect to attain this 7–9 cm level of consistency when we calculate RMS(SSH − ⟨DOT⟩ − geoid). Though slightly larger than this level in the north, and about 1 cm larger in the south, we do indeed find that including the ⟨DOT⟩ significantly decreases the residual (black lines in Figure 3) and does reach the desired level when the geoid correction field is applied (not shown). For these calculations $\langle DOT_{SE} \rangle$ and $\langle DOT_{AV} \rangle$ reach similar levels of consistency. Though the differences are subtle, the black lines in Figure 3 show that $\langle DOT_{AV} \rangle$ performs slightly better in the northern domain, while $\langle DOT_{SE} \rangle$ performs slightly better in the southern domain, reinforcing our previous assertion of uncertainty levels in the ⟨DOT⟩.

4.3. Residuals r_i and r_c After Accounting for the Time-Varying DOT

Regardless of uncertainty levels, the above RMS calculations are not expected to yield vanishing residuals as they specifically retain eddy variability in the ocean. In three further calculations we take eddies into account and hypothesize that the residuals should be negligible. The first calculation, RMS(SSH − DOT'_{AV} − DTU10), includes the time-varying mapped dynamic ocean topography determined from altimetry, DOT'_{AV}. (For this calculation only, however, DOT'_{AV} is referenced to the 1993 to 2009 period in consistency with the time period over which the DTU10 product was determined.) This RMS calculation omits uncertainties in the geoid but introduces uncertainties in DTU10, uncertainties in DOT'_{AV}, and uncertainties due to any inconsistencies in the processing of the DTU10 and AVISO products. The RMS residuals for this calculation are approximately 4 cm in both the northern and southern domains (lower green line in Figure 3). If DTU10 was exactly equal to ⟨SSH⟩, then this would be a check on how well DOT'_{AV} accounts for the temporal variability in the along-track SSH and thus be a floor for the expected r_c.

We calculate RMS(SSH − DOT_{AV} − geoid) and find a value of ∼5 cm. This increase of ∼1 cm reflects what we saw above: that the mapped DTU10 is more consistent with SSH measurements than is the mean sea surface implied by (⟨DOT_{AV}⟩ + geoid). However, when we add our calculated geoid correction, we find that RMS(SSH − DOT_{AV} − geoid − F_{AV}) reaches this same level of consistency in the northern domain and becomes significantly closer in the southern domain. If we neglect depths shallower than 1000 m in this calculation, we reach the desired 4 cm level of consistency in the southern domain (not shown). As expected, since ⟨DOT_{SE}⟩ + F_{SE} is approximately equal to ⟨DOT⟩$_{AV}$ + F_{AV}, we find the same results for the calculation of RMS(SSH − ⟨DOT⟩$_{SE}$ − DOT'_{AV} − geoid − F_{SE}). Thus, much of the discrepancy between DTU10 and (⟨DOT⟩ + geoid) was due to errors in the geoid that we were able to account for with F.

5. Oceanographic Utility of the Correction Field

SSH anomalies from Jason class altimeters have approximately 3 cm uncertainties [*Ponte et al.*, 2007]. We find that the combined altimeter and EGM2008 error is approximately ∼6 cm in this region as deduced from the upper red line in Figure 3. The Jason repeat altimeters imply, however, that there are local regions where the mean misfit between SSH, geoid, and DOT exceeds 15 cm. Using this information, we made a correction field (section 3). This correction reduces the combined uncertainty over the region to ∼5 cm (lower red line in Figure 3).

Figure 3 shows that correcting a gridded geoid product with information from repeat altimeter missions allows better use of nonrepeat altimeters. Oceanographic assimilations rely primarily, if not solely, on repeat altimeters. They use SSH anomalies that are not affected by geoid uncertainties. For example, Jason-2 has a repeat period of 9.9 days. An assimilation window of 1 month will have three constraints at every along-track location: one mean constraint with an error variance that will be the combined altimeter and geoid error (e.g., 6 cm) and two anomaly constraints with error variance equal to the altimeter error alone (e.g., 3 cm). CryoSat-2 has a repeat cycle of 369 days. The example assimilation will contain many CryoSat-2 measurements, but they will mostly not be collocated in space. The utility of this high-precision altimeter will therefore be degraded as every one of the measurements will carry the combined altimeter and geoid uncertainty. Mapping a geoid correction, as we have done, propagates the geoid correction information provided by the repeat altimeters. The result is that the prescribed uncertainty on the CryoSat-2 constraint can be reduced. Including all altimeters in the mapping, which we have yet to do, could further refine the spatial structure of the geoid correction.

To emphasize the oceanographic value, we show the residual between the AVISO DOT, EGM2008, and CryoSat-2, r_i = SSH_{C2} − DOT_{AV} − geoid, for the arbitrarily chosen month of July 2012 (Figure 2c). These data were not used in deriving the correction. There are locations of large misfit throughout the region and especially off the coast of Northern California where the residual is systematically negative. After the geoid correction is applied, the residual misfit, r_c = SSH_{C2} − DOT_{AV} − geoid − F_{AV}, becomes shorter scale and the RMS is reduced from 6.7 cm to 5.6 cm over the domain shown in Figures 2c and 2d. Shoreward of the black line in the figure the RMS is reduced from 9.2 cm to 7.3 cm. The correction gives greater confidence that remaining residual errors are primarily from the DOT estimate. Therefore, we conclude that data-model syntheses with short assimilation windows, or other analytic methods, can use the procedure described in this paper to reduce the prescribed error variance on altimeters with long repeat periods.

6. Discussion and Conclusions

Satellite gravity mapping missions, altimeters, and other platforms have allowed the Earth's geoid to be mapped over the ocean to a horizontal resolution of approximately 100 km with an uncertainty of less than 10 cm. For finer resolution, with the exception of a few specific geographic regions, this uncertainty increases to greater than 10 cm [*Bingham et al.*, 2014]. To achieve greater accuracy requires accurate estimates of the dynamic ocean topography. Here we solve for a geoid correction for the region of the California Current System using two dynamic ocean topography estimates that have uncertainties less than 10 cm. With this correction we improve the overall consistency with along-track altimetric observations in the region by about 1 cm. While this is a modest improvement, it validates the assertion that the derived field is a correction to the gravitational field. Furthermore, this correction is as large as the dynamic ocean topography itself, with magnitude ∼15 cm and a RMS of ∼3 cm, and significant structure, especially near the coast. This result is evidence that modern high-resolution dynamic ocean topography products, which are inferred by combining known physics with observations, can inform geoid models.

A future effort is to assign error bars to DOT inferences, which will remove ambiguity in geoid correction fields. Additionally, this will allow a better combination of products (e.g., a state estimate ⟨DOT⟩ with the AVISO mapped DOT′). Assigning useful model error covariances is not a trivial task. One way to validate the a priori assigned error covariance is to use assimilation a posteriori to determine consistency of the inferred geoid correction with model physics and other observational constraints.

The geoid correction determined here could be improved by advancing our knowledge of the uncertainty structure in the altimeter measurements. This includes uncertainty with respect to the applied corrections, for example, to account for atmospheric water vapor content, ocean tides, and ocean sea state. Here we only used the Jason altimeters to derive the geoid correction. Using all altimeter measurements would also improve the geoid correction. Perhaps most importantly, however, the geoid correction map would be improved if we had more information on geoid error. We found that there was significant geoid error variance that was apparently correlated with topographic structure. The correlation was not tight, and in this work we accounted for this by increasing the prescribed SSH uncertainty. The relationship between topography and geoid error certainly deserves further investigation. The uncertainty estimates used in this work need improvement; nevertheless, our results do make clear that we are able to identify locations where geoid models need improvement (Figures 2a and 2b), and we suggest that the method be applied to other regions to benefit geodesists and oceanographers alike.

Acknowledgments

Support for this work was provided by the National Geospatial-Intelligence Agency (NGA), NGA University Research Initiative (NURI) grant HM1582-10-1-0003. The authors thank the data providers (all data sources listed in text). The authors thank Nikos Pavlis for providing the mapped EGM2008 and for helpful comments on this manuscript. The authors also thank the anonymous reviewers. B. C. was funded by the Climate Observations and Monitoring Program, National Oceanic and Atmospheric Administration, U.S. Department of Commerce. The views expressed herein are those of the authors and do not necessarily reflect the views of NOAA.

The Editor thanks two anonymous reviewers for their assistance in evaluating this paper.

References

Andersen, O. B., and P. Knudsen (2009), DNSC08 mean sea surface and mean dynamic topography models, *J. Geophys. Res.*, *114*, C11001, doi:10.1029/2008JC005179.

Bingham, R. J., K. Haines, and D. J. Lea (2014), How well can we measure the ocean's mean dynamic topography from space?, *J. Geophys. Res. Oceans*, *119*, 3336–3356, doi:10.1002/2013JC009354.

Davis, R., M. D. Ohman, D. L. Rudnick, J. T. Sherman, and B. A. Hodges (2008), Glider surveillance of physics and biology in the southern California Current System, *Limnol. Oceanogr.*, *53*(5, part 2), 2151–2168.

Ducet, N., P. Y. Le Traon, and G. Reverdin (2000), Global high-resolution mapping of ocean circulation from TOPEX/Poseidon and ERS-1 and -2, *J. Geophys. Res.*, *105*, 19,477–19,498, doi:10.1029/2000JC900063.

Ganachaud, A., C. Wunsch, M.-C. Kim, and B. Tapley (1997), Combination of TOPEX/Poseidon data with a hydrographic inversion for determination of the oceanic general circulation and its relation to geoid accuracy, *Geophys. J. Int.*, *128*(3), 708–722, doi:10.1111/j.1365-246X.1997.tb05331.x.

Gay, P. S., and T. K. Chereskin (2009), Mean structure and seasonal variability of the poleward undercurrent off Southern California, *J. Geophys. Res.*, *114*, C02007, doi:10.1029/2008JC004886.

Hughes, C. W., and R. J. Bingham (2008), An oceanographer's guide to GOCE and the geoid, *Ocean Sci.*, *4*(1), 15–29, doi:10.5194/os-4-15-2008.

Knudsen, P., R. Bingham, O. Andersen, and M.-H. Rio (2011), A global mean dynamic topography and ocean circulation estimation using a preliminary GOCE gravity model, *J. Geod.*, *85*(11), 861–879, doi:10.1007/s00190-011-0485-8.

Lynn, R. J., and J. J. Simpson (1987), The California Current System: The seasonal variability of its physical characteristics, *J. Geophys. Res.*, *92*(C12), 12,947–12,966, doi:10.1029/JC092iC12p12947.

Marshall, J., A. Adcroft, C. Hill, L. Perelman, and C. Heisey (1997), A finite-volume, incompressible Navier-Stokes model for studies of the ocean on parallel computers, *J. Geophys. Res.*, *102*(C3), 5753–5766.

Maximenko, N., P. Niiler, L. Centurioni, M.-H. Rio, O. Melnichenko, D. Chambers, V. Zlotnicki, and B. Galperin (2009), Mean dynamic topography of the ocean derived from satellite and drifting buoy data using three different techniques*, *J. Atmos. Oceanic Technol.*, *26*(9), 1910–1919, doi:10.1175/2009JTECHO672.1.

Nerem, R. S., B. D. Tapley, and C. K. Shum (1990), Determination of the ocean circulation using Geosat altimetry, *J. Geophys. Res.*, *95*(C3), 3163–3179, doi:10.1029/JC095iC03p03163.

Ohman, M., et al. (2013), Autonomous ocean measurements in the California Current Ecosystem, *Oceanography*, *26*(3), 18–25.

Pail, R., et al. (2011), First GOCE gravity field models derived by three different approaches, *J. Geod.*, *85*(11), 819–843, doi:10.1007/s00190-011-0467-x.

Pavlis, N. K., S. A. Holmes, S. C. Kenyon, and J. K. Factor (2012), The development and evaluation of the Earth Gravitational Model 2008 (EGM2008), *J. Geophys. Res.*, *117*, B04406, doi:10.1029/2011JB008916.

Ponte, R. M., C. Wunsch, and D. Stammer (2007), Spatial mapping of time-variable errors in *Jason*-1 and TOPEX/Poseidon sea surface height measurements, *J. Atmos. Oceanic Technol.*, *24*, 1078–1085.

Rapp, R. H. (1998), Past and future developments in geopotential modeling, in *Geodesy on the Move: Gravity, Geoid, Geodynamics and Antarctica, IAG Symposia*, vol. 119, edited by R. Forsberg, M. Feissel, and R. Dietrich, pp. 58–78, Springer, Berlin.

Rio, M. H., S. Guinehut, and G. Larnicol (2011), New CNES-CLS09 global mean dynamic topography computed from the combination of GRACE data, altimetry, and in situ measurements, *J. Geophys. Res.*, *116*, C07018, doi:10.1029/2010JC006505.

Stammer, D., C. Wunsch, R. Giering, C. Eckert, P. Heimbach, J. Marotzke, A. Adcroft, C. N. Hill, and J. Marshall (2002), Global ocean circulation during 1992–1997, estimated from ocean observations and a general circulation model, *J. Geophys. Res.*, *107*(C9), 3118, doi:10.1029/2001JC000888.

Tai, C. K., and C. Wunsch (1983), Absolute measurement by satellite altimetry of dynamic topography of the Pacific Ocean, *Nature*, *301*(5899), 408–410.

Tapley, B. D., D. P. Chambers, S. Bettadpur, and J. C. Ries (2003), Large scale ocean circulation from the GRACE GGM01 Geoid, *Geophys. Res. Lett.*, *30*(22), 2163, doi:10.1029/2003GL018622.

Todd, R. E., D. L. Rudnick, M. R. Mazloff, R. E. Davis, and B. D. Cornuelle (2011), Poleward flows in the southern California Current System: Glider observations and numerical simulation, *J. Geophys. Res.*, *116*, 2156–2202, doi:10.1029/2010JC006536.

Todd, R. E., D. L. Rudnick, M. R. Mazloff, B. D. Cornuelle, and R. E. Davis (2012), Thermohaline structure in the California current system: Observations and modeling of spice variance, *J. Geophys. Res.*, *117*, C02008, doi:10.1029/2011JC007589.

Verdy, A., M. R. Mazloff, B. D. Cornuelle, and S. Y. Kim (2014), Wind-driven sea level variability on the california coast: An adjoint sensitivity analysis, *J. Phys. Oceanogr.*, *44*(1), 297–318.

Volkov, D., and V. Zlotnicki (2012), Performance of GOCE and GRACE-derived mean dynamic topographies in resolving Antarctic Circumpolar Current fronts, *Ocean Dyn.*, *62*(6), 893–905, doi:10.1007/s10236-012-0541-9.

Wunsch, C., and E. M. Gaposchkin (1980), On using satellite altimetry to determine the general circulation of the oceans with application to geoid improvement, *Rev. Geophys.*, *18*(4), 725–745, doi:10.1029/RG018i004p00725.

Wunsch, C., and P. Heimbach (2013), Chapter 21—Dynamically and kinematically consistent global ocean circulation and ice state estimates, in *Ocean Circulation and Climate: A 21st Century Perspective, International Geophysics*, vol. 103, edited by C. Wunsch and P. Heimbach, pp. 553–579, Acad. Press, Cambridge, Mass., doi:10.1016/B978-0-12-391851-2.00021-0.

Zlotnicki, V., and J. G. Marsh (1989), Altimetry, ship gravimetry, and the general circulation of the North Atlantic, *Geophys. Res. Lett.*, *16*, 1011–1014.